Supporting Information

In-situ Construction of Core-shell Structured Cobalt Oxide @ Nickel-Cobalt-Layered Double Hydroxide Nanorods with Abundant Oxygen Vacancies Towards Boosting Electrochemical Energy Storage

Xiao-Man Cao,[‡] Di Liu,[‡] Zhi-Jia Sun,* and Qingguo Zhang*

College of Chemistry and Materials Engineering, Bohai University, Jinzhou 121013, P.R. China.
E-mail: sunzhijia@bhu.edu.cn; zhangqingguo@bhu.edu.cn

[‡]These authors contributed equally to this work.

1 Experimental section

1.1 Materials

The chemicals in the experiments were analytical grade and were used without any further purification. Cobalt nitrate ($Co(NO_3)_2 \cdot 6H_2O$, ≥99%), ammonium fluoride (NH_4F, ≥99%), urea (CH_4N_2O, ≥99%), 2-methylimidazole ($C_4H_6N_2$, ≥99%), nickel nitrate ($Ni(NO_3)_2 \cdot 6H_2O$, ≥99%), H_2O_2 were purchased from Sinopharm Chemical Reagent, and ethanol were purchased from Shanghai Macklin Biochemical Co., Ltd. Nickel foam (NF) was purchased from Tian He Cheng Technology Co., Ltd.

1.2 Preparation of NC

Ni foam was pretreated by ultrasonication with ethanol and deionized water for 15 min respectively to ensure a clean surface. To ensure complete dissolution, $Co(NO_3)_2 \cdot 6H_2O$, (135 mg), urea, (135 mg), and NH_4F, (66.6 mg) were dissolved in 9 mL of deionized water and agitated for 30 min. The reaction solution was then added to a 20 mL Teflon-lined stainless-steel autoclave, into which a prepared piece of Ni foam (1×1 cm^2, ca. 25 mg) was dipped. The autoclave was heated to 120 ^{o}C for 10 h. The precursor (Co(OH)F) was cooled to room temperature, washed numerous times with deionized water and ethanol, and then dried at 60 ^{o}C for 2 h. Finally, all samples were arranged vertically in the alumina boat, transferred to a tube furnace, and annealed for 1 h at 450 ^{o}C h in an Ar atmosphere with a heating rate of 4 ^{o}C min^{-1} before being cooled to ambient temperature to obtain a tawny sample known as NC.

1.3 Preparation of NCM

2.5 mL of deionized water and 0.82 g of 2-methylimidazole were dissolved, followed by the addition of 2.5 mL of ethanol and another 15 min of ultrasound. After that, the sample was immersed in the combined solution for 24 h at room temperature in a sealed glass vial. The sample was then dried for a whole night at 80 ^{o}C after being rinsed numerous times with anhydrous ethanol. The name of the sample was NCM, and the color turned purple as a result.

1.4 Preparation of NCLO

5 mmol of $Ni(NO_3)_2 \cdot 6H_2O$ was dissolved in 10 mL of deionized water and ultrasonic

mixing for 15 min to obtain a green solution. The NCM was then impregnated with the green solution, and the reaction took place there for 36 h. After numerous rounds of washing with deionized water and drying at 80 °C overnight, NCL is obtained and the color of the sample changing from purple to green. Finally, NCLO was produced by soaking the NCL electrode in 0.07% H_2O_2 for 1 min. The mass loading of CoO@Ov-NiCo LDH on Ni foam substrate is about 2 mg cm^{-2}.

1.5 Materials characterization

The microstructure and morphology of samples were studied by scanning electron microscopy (SEM) using a Hitachi S-4800 system and transmission electron microscopy (TEM) using a Hitachi JEM-2100 system, and energy-dispersive spectroscopy (EDS) was performed using a SEM instrument (Oxford Instruments). The powder X-ray diffraction (PXRD) pattern was collected by using a Bruker AXS D8 system within the scanning range from 5 to 85° at a voltage of 40 kV and a current of 40 mA with Cu-α radiation (λ = 1.5406 Å). X-ray photoelectron spectroscopy (XPS) was performed on a Thermo ESCALAB 250 with Al-Kα ($h\nu$ = 1486.6 eV). In situ electron paramagnetic resonance (EPR) measurement was taken in an endor spectrometer (JEOL ES-ED3X). The pore structure and specific surface area of samples were characterized by using N_2 adsorption–desorption isotherms at 77 K using a Kubo X1000 system. The mass loading of the active materials was measured using an analytical balance (BT 25 S, Sartorius, Germany, sensitivity: 0.01 mg). The electrochemical properties of the electrodes were conducted using a CHI electrochemical workstation (660E, ChenHua, China).

2 Calculations section

2.1 Calculations of single electrode

At room temperature, all samples were put into 6 M KOH aqueous electrolyte and performed the electrochemical properties by using a three-electrode system connected to electrochemical workstation CHI660E (Chen Hua, Shanghai, China), and a Pt foil and a Hg/HgO electrode as the counter and reference electrodes respectively. The area-specific capacitance of a single electrode can be calculated based on galvanostatic charge-discharge experiments according to following equation (1)-(2):

$$C_a = \frac{I \times t}{\Delta V \times S} \tag{1}$$

$$C_{sa} = \frac{2I \int Vdt}{mV} \tag{2}$$

Where C_s (F cm^{-2}) and C_{ma} (mAh g^{-1}) are the area-specific capacitance, I is the discharge current (A), t is the time (s), ΔV is the potential window (V) and S is the area of electrode (cm^2) and $\int Vdt$ is the integral area under the discharge curve.

The mass-specific capacitance of a single electrode can be calculated based on galvanostatic charge-discharge experiments according to following equation (3)-(4):

$$C_m = \frac{I \times t}{\Delta V \times m} \tag{3}$$

$$C_{ma} = \frac{2I \int Vdt}{mV} \tag{4}$$

Where C_m (F g^{-1}) and C_{ma} (mAh g^{-1}) are the mass-specific capacitance, I is the discharge current (A), t is the time (s), ΔV is the potential window (V), m is the mass of active material (g) and $\int Vdt$ is the integral area under the discharge curve.

The determination of the electrochemically active surface area (ECSA) using the following equation (5):

$$ECSA = \frac{C_{dl}}{C_s}$$

(5)

Where C_s represents the general specific capacitance of a smooth standard electrode with a surface area of 1 cm^{-2}. C_{dl} represents the electric double-layer capacitance value and can be calculated by evaluating the relationship between the scan rate and the difference between the anodic and cathodic current densities in the non-faradaic area. A comparison of the NCL and NCLO electrodes is shown in Fig. S6.

The charge storage mechanism of NCLO was explored by using the following equation (6)-(7):

$$i = av^b$$

(6)

$$log\ i = b\ log\ v + log\ a$$

(7)

Where a and b represent adjustable values and i represent the peak current (A), v represents the scan rate (mV s^{-1}). The b value approaching 0.5 represents that the charge storage mechanism is dominated by a traditional diffusion-controlled process. When the b value is close to 1.0, the reaction is mainly controlled by the surface capacitance process. For b values between 0.5 and 1.0, the charge storage process presents a mixed mechanism.

The contribution ratio of diffusion control and surface control to the capacitance of NCLO was calculated by using the following equation (8)-(9):

$$i = k_1 v + k_2 v^{1/2}$$

(8)

$$i/v^{1/2} = k_1 v^{1/2} + k_2$$

(9)

Where i is the current (A), and k_1 and k_2 are constants. Based on the linear relation of $i/v^{1/2}$ and $v^{1/2}$, k_1 and k_2 are calculated at different scan rates from 2 to 10 mV s^{-1}.

2.2 Capacitances of ASC Devices

In order to obtain better electrochemical performance of the device, according to charge balance following the relationship $Q_+ = Q_-$ of positive electron and negative electron, the mass rate of electron was calculated by following equations (10)-(12):

$$Q = C_m \times \Delta V \times m \tag{10}$$

$$Q_+ = Q_- \tag{11}$$

$$\frac{m^+}{m^-} = \frac{C^- \times \Delta V^-}{C^+ \times \Delta V^+} \tag{12}$$

Where Q is capacity, C_m represents specific capacitance of electrode materials, m is the mass of active materials (g). C^+ and ΔV^+ denote specific capacitance and potential window of positive electrode. At the same time, C^- and ΔV^- denote specific capacitance and potential window of negative electrode.

The area-specific capacitance (C_S, F cm^{-2}) of ASC device can be calculated based on galvanostatic charge-discharge experiments according to equation (13):

$$C_S = \frac{I \times t}{\Delta V \times S} \tag{13}$$

Where I is the discharge current (A), t is the discharge time (s), ΔV is the operating voltage of the ASC (V) and S is the area of electrode (cm^2).

The mass-specific capacitance (C_M, F g^{-1}) and (C_{Ma}, mAh g^{-1}) of ASC device can be calculated based on galvanostatic charge-discharge experiments according to equation (14)-(15):

$$C_M = \frac{I \times t}{\Delta V \times M} \tag{14}$$

$$C_{Ma} = \frac{2I \int V dt}{MV} \tag{15}$$

Where I is the discharge current (A), t is the discharge time (s), ΔV is the potential

window (V) and M is the total mass of active materials (g) and $\int Vdt$ is the integral area under the discharge curve.

2.3 Energy Density and Power Density of ASC Device

The mass-specific energy density (E_M, Wh kg^{-1}) and power density (P_M, W kg^{-1}) of the device are calculated using the following equations (16)-(17):

$$E_M = \frac{1000 \times C_M \times \Delta V^2}{2 \times 3600} \tag{16}$$

$$P_M = \frac{3600 \times E_M}{\Delta t} \tag{17}$$

Where ΔV denotes potential window during the discharge process (V), C_M represents specific capacitance of the device (F g^{-1}) and Δt is discharge time of galvanostatic charge-discharge (s).

2.4 Density function theory calculations

All computations were performed by density functional theory (DFT). The electron exchange and correlation energy were calculated by the Perdew-Burke-Ernzerhof (PBE) functional with a generalized gradient approximation (GGA).[1] A 4×2×1 Monkhorst-Pack k-point sampling of the Brillouin zone was adopted for the structure optimization and electronic property calculations.[2] The kinetic cutoff energy for plane-wave basis set was set as 600 eV. The total energy and force convergence were set to be smaller than 10^{-5} eV and 0.02 eV Å^{-1}, respectively.
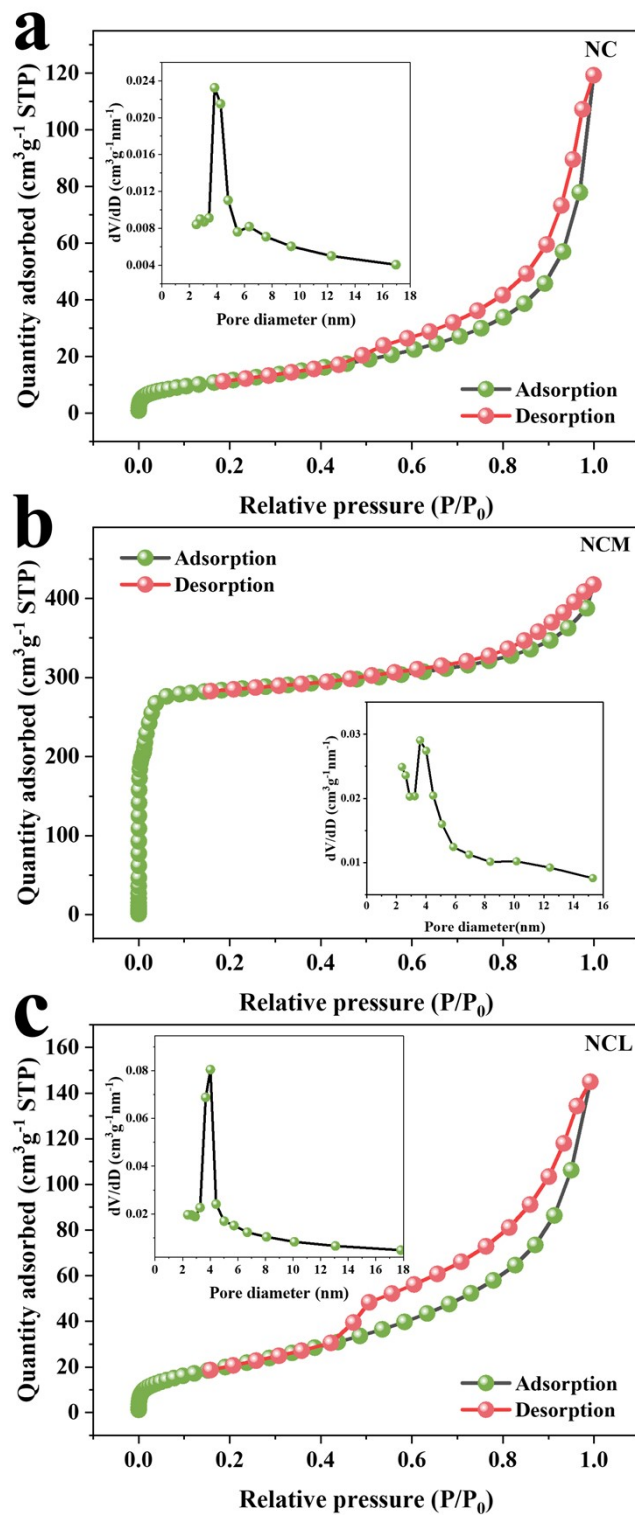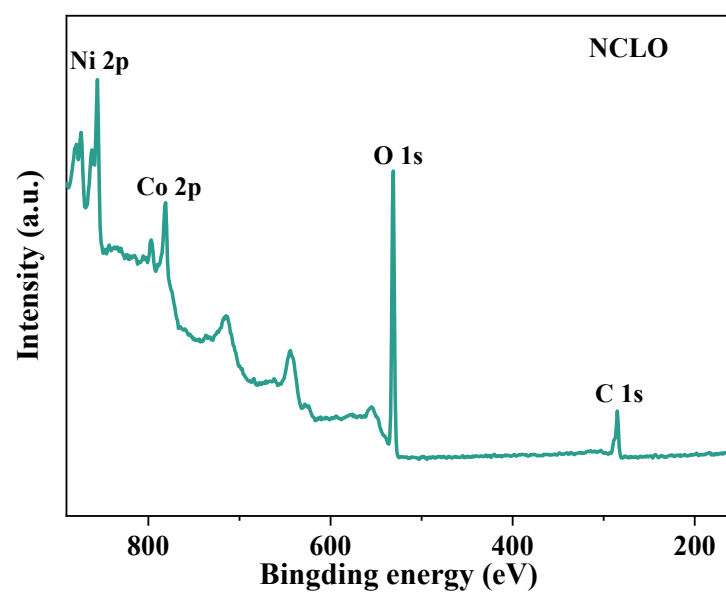
3. Supplementary Figure and Tables
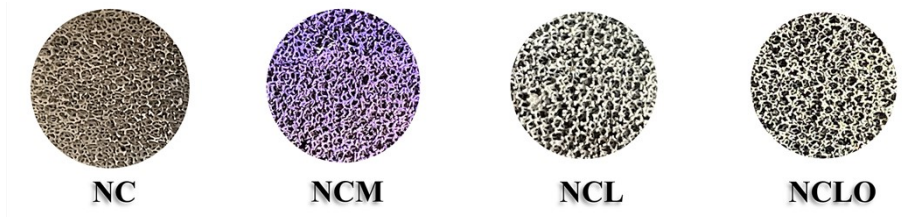
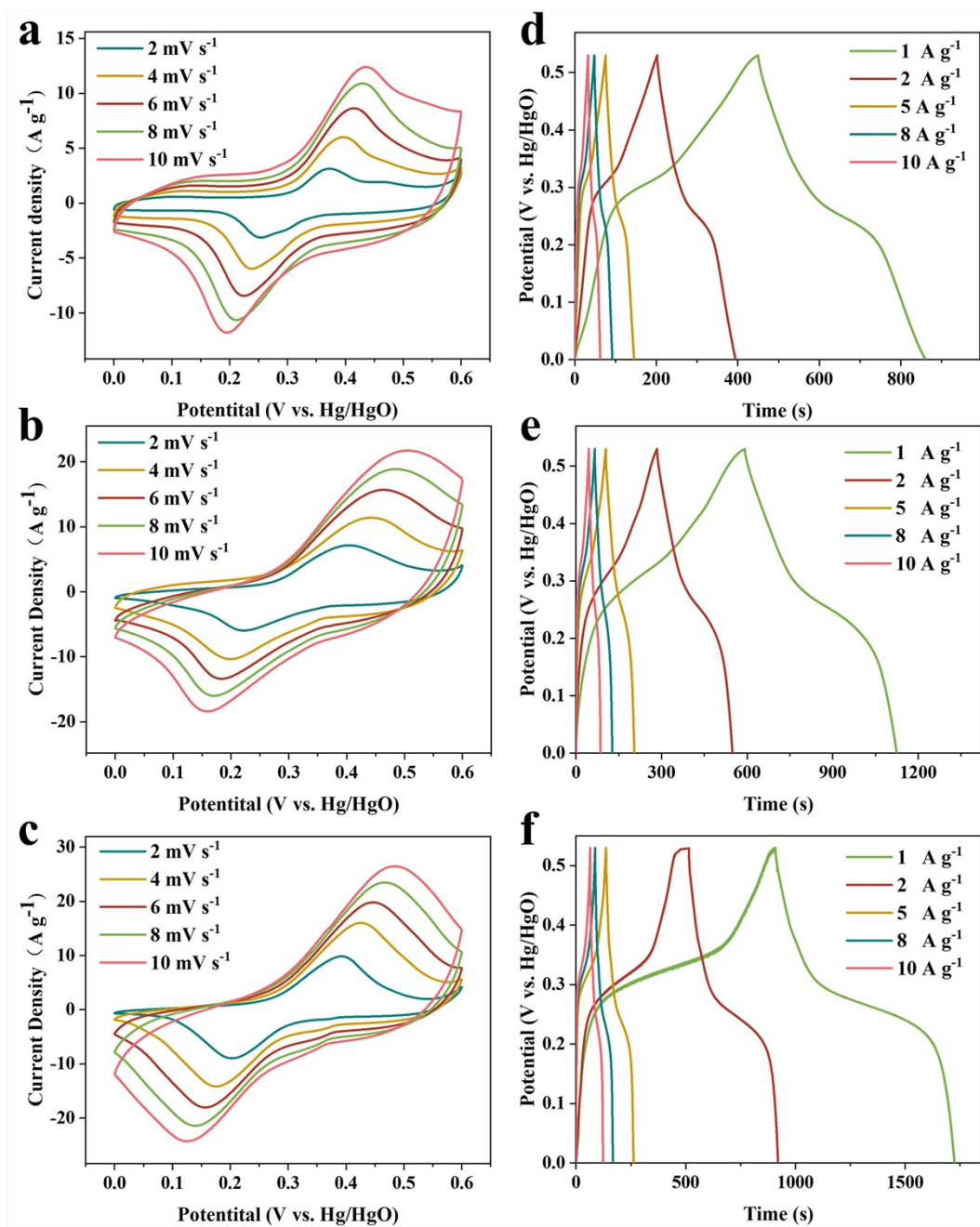**Fig. S1** Photos of NC, NCM, NCL, NCLO.
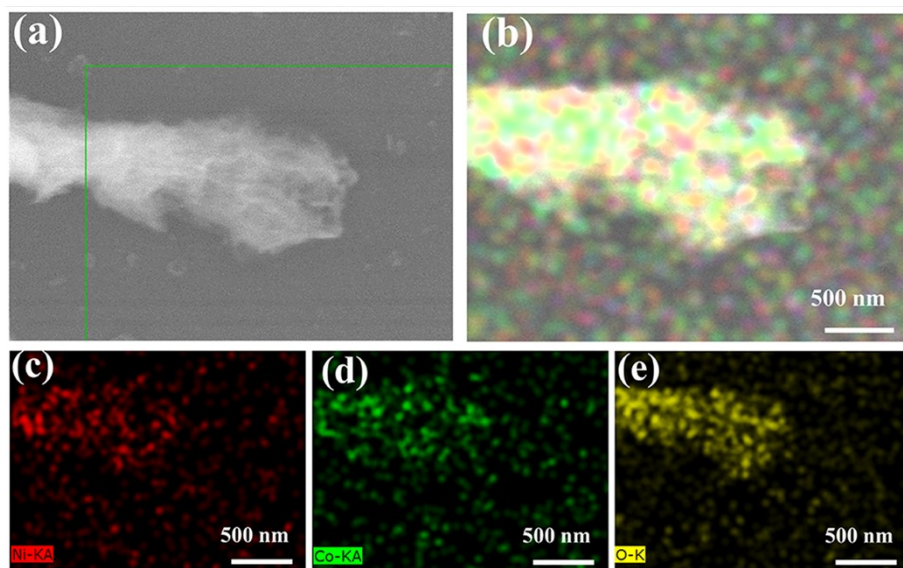
Fig. S2 SEM image of NCLO (a) and corresponding EDS elemental mapping of Ni, Co, O (b-e).

Fig. S3 Nitrogen (77K) adsorption-desorption isotherms and pore size distribution for
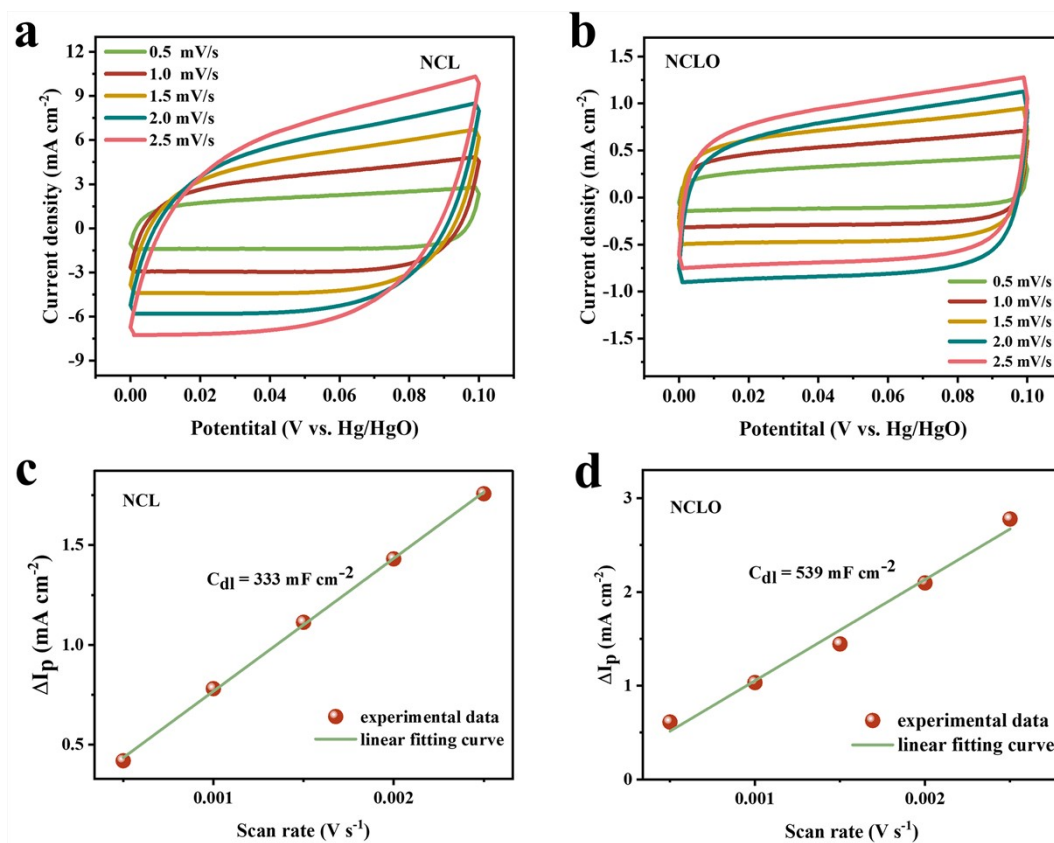(a) NC, (b) NCM and (c) NCL.

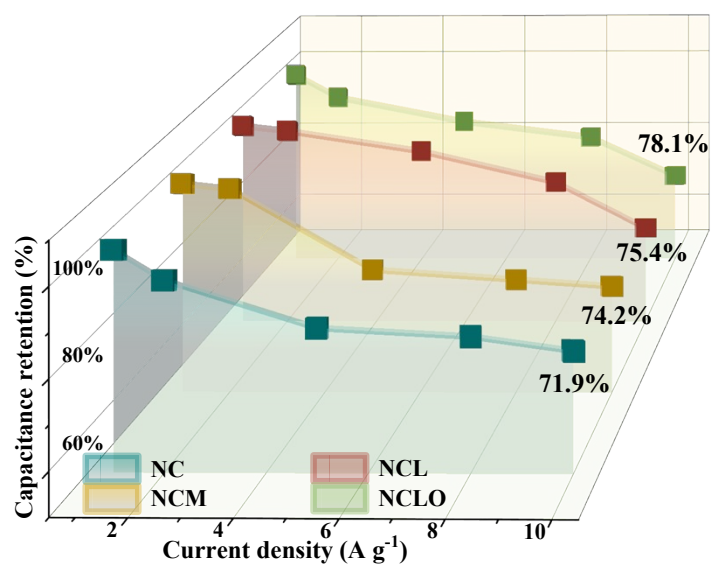**Fig. S4** XPS survey spectrum of NCLO.

Fig. S5 CV curves of (a) NC, (b) NCM, (c) NCL; GCD curves of (d) NC, (e) NCM, (f) NCL.
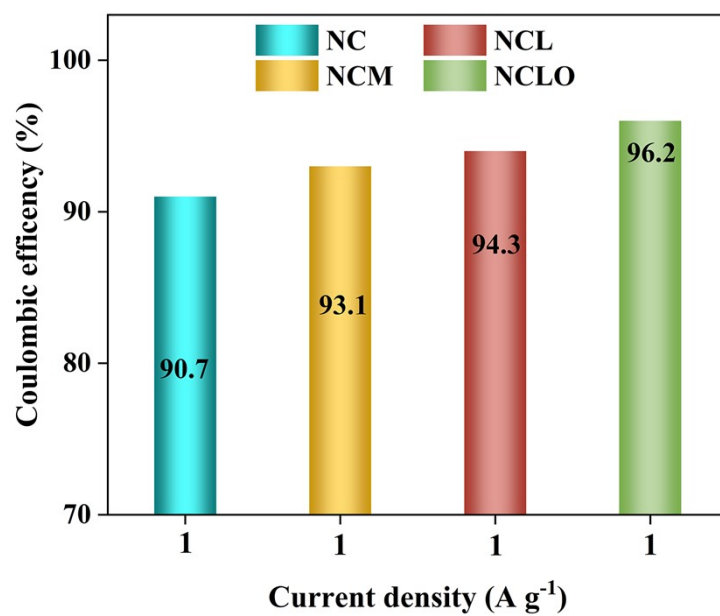
Fig. S6 CV curves of (a) NCL and (b) NCLO in the non-faradic region; (c) and (d) the corresponding total electrochemically active surface area evaluation.

Fig. S7 Capacitance retention of NC, NCM, NCL, NCLO at different current densities of 1-10 A g^{-1}.
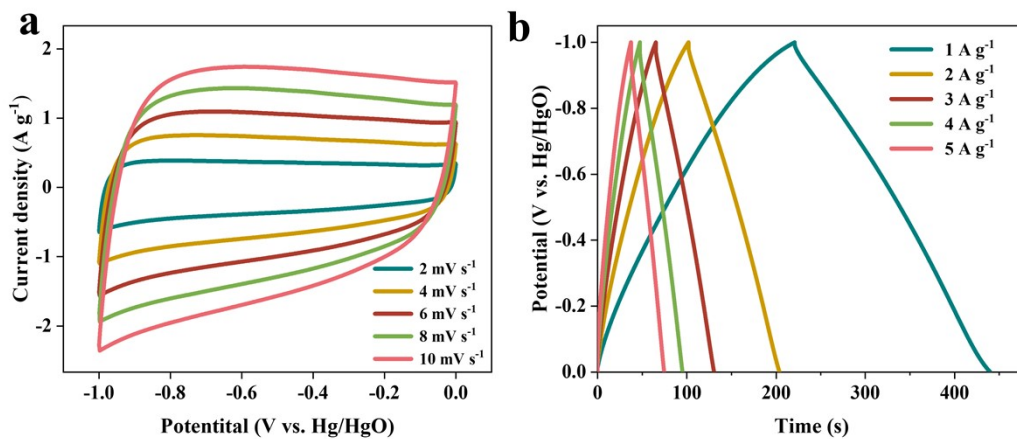
Fig. S8 Coulomb efficiency of NC, NCM, NCL, NCLO at current densities of 1 A g^{-1}.
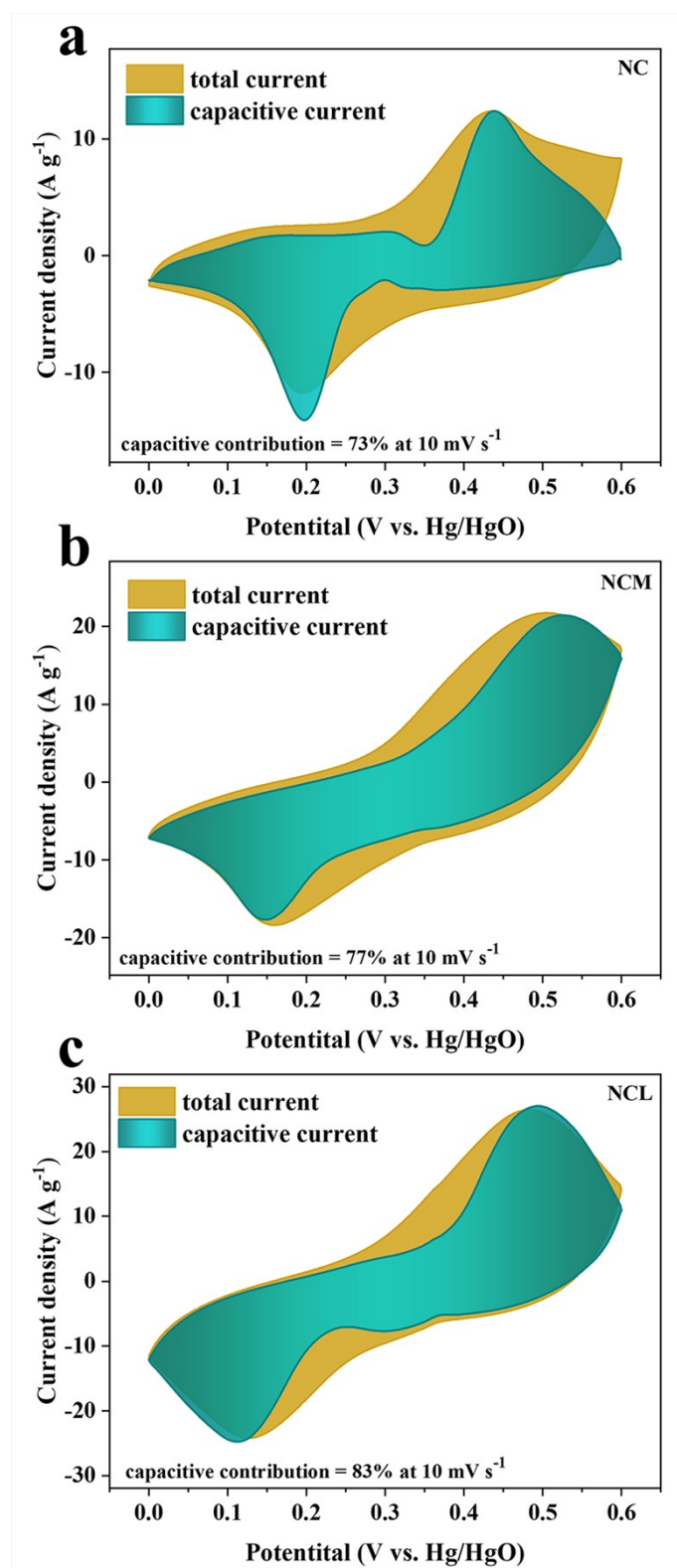
Fig. S9 Contributions of (a) NC, (b) NCM, (c) NCL electrode that are controlled by diffusion and capacitance for charge storage.

Fig. S10 (a) CV curves of AC at different scan rates from 2 to 10 mV s^{-1}; (b) GCD curves of AC at different current densities from 1 to 5 A g^{-1}.

Table S1. specific surface for NC, NCM, NCL and NCLO.

	NC	NCM	NCL	NCLO
specific surface ($m^2\,g^{-1}$)	43	880	68	94

Table S2. O1s peak area ratio of NCL and NCLO calculated from XPS spectra.

	O_W	O_V	O_{OH}	O_L
NCL	1.04%	20.14%	46.79%	32.03%
NCLO	1.19%	31.74%	42.09%	24.98%

Table S3. The ratio of Ni^{2+}/Ni^{3+} and Co^{2+}/Co^{3+} in NCL and NCLO calculated from XPS spectra.

	Ni^{2+}/Ni^{3+}	Co^{2+}/Co^{3+}
NCL	1.24	2.43
NCLO	1.78	1.77

Table S4. Comparison of specific capacitance of NCLO with various Ni/Co based electrodes materials

Type	Morphology	Electrolyte	Current density	Capacitance	Ref.
NiCo$_2$S$_4$@NiFe LDH	Nanosheets	3 M KOH	1 A g^{-1}	827 F g^{-1}	[3]
Co(OH)$_2$@CoNi LDH/3D-Ni/CNW	Nanoworms	2 M KOH	1 A g^{-1}	996 F g^{-1}	[4]
NiMn-LDH	Hollow sphere	3 M KOH	0.2 A g^{-1}	1010 F g^{-1}	[5]
NiV-LDHs	Ball-flower	6 M KOH	1 A g^{-1}	1069 F g^{-1}	[6]
Ni-Co LDH@Co$_3$O$_4$ Nc	Nanocubes	1 M KOH	2 A g^{-1}	1866 F g^{-1}	[7]
NiCo(NA)-LDH@ACC	Nanosheets	6 M KOH	0.62 A g^{-1}	1709 F g^{-1}	[8]
Co$_3$O$_4$@NiCoLD HNSs	Nanosheets	1 M KOH	1 A g^{-1}	1708 F g^{-1}	[9]
NiCo-LDH@NCF	Nanosheets	2 M KOH	0.5 A g^{-1}	756 F g^{-1}	[10]
NCLO	**Nanorod**	**6 M KOH**	**1 A g^{-1}**	**2264.2 F g^{-1}**	**This work**

Table S5. The fitting results of R_s and R_{ct} for NC, NCM, NCL, NCLO electrodes.

Electrodes	NC	NCM	NCL	NCLO
R_s	0.631 Ω	0.712 Ω	0.552 Ω	0.548 Ω
R_{ct}	0.760 Ω	0.920 Ω	1.81×10^{-4} Ω	5.56×10^{-5} Ω

Table S6. The comparative electrochemical performance for ASCs based on the Ni/Co electrodes.

Device	Window (V)	Electrolyte	Energy density (Wh kg^{-1})	Power density (W kg^{-1})	Ref.
ZNC/CWO-10//AC	1.8	2 M KOH	17.41	181.2	[11]
Vo-NiCo LDH//Fe$_2$O$_3$	1.3	3 M KOH	19.5	430	[12]
NCNRs@NCNSs//AC	1.5	6 M KOH	22.81	375	[13]
Co$_3$O$_4$@Ni-Co LDH//AC	1.6	2 M KOH	46.3	64.2	[14]
CuCo$_2$O$_4$@Ni$_{0.5}$Co$_{0.5}$(OH)$_2$//AC	1.6	KOH-PVA	32	800	[15]
D-NiCo-LDH/NF//AC	1.5	3 M KOH	53	752	[16]
NCLO//AC	**1.6**	**6 M KOH**	**63.8**	**800.0**	**This work**

References

1 J. P. Perdew, K. Burke and M. Ernzerhof, Generalized Gradient Approximation Made Simple, *Phys. Rev. Lett.*, 1996, **77**, 3865–3868.

2 H. J. Monkhorst and J. D. Pack, Special points for Brillouin-zone integrations, *Phys. Rev. B*, 1976, **13**, 5188–5192.

3 S. S. Rabbani, H. Mustafa, A. Zafar, S. Javaid, M. A. Bakar, A. Nisar, Y. Liu, S. Karim, H. Sun, S. Hussain, Z. Zafar, Y. Faiz, F. Faiz, Y. Yu and M. Ahmad, Nickel foam supported hierarchical $NiCo_2S_4$@NiFe LDH heterostructures as highly efficient electrode for long cycling stability supercapacitor, *Electrochim Acta*, 2023, **446**, 142098.

4 A. Sharifi, M. Arvand and S. Daneshvar, Flexible Fiber-Shaped Supercapacitor Based on Hierarchically $Co(OH)_2$ Nanosheets@NiCo LDH Nanoworms/3D-Ni Film Coated on the Binary Metal Wire Substrate for Energy Storage Application, *J Inorg Organomet Polym*, 2023, **33**, 761–770.

5 J. Kumar, R. R. Neiber, Z. Abbas, R. A. Soomro, A. BaQais, M. A. Amin and Z. M. El-Bahy, Hierarchical NiMn-LDH Hollow Spheres as a Promising Pseudocapacitive Electrode for Supercapacitor Application, *Micromachines*, 2023, **14**, 487.

6 Q. Tu, Q. Zhang, X. Sun, J. Wang, B. Lin, L. Chen, J. Liu and Z. Deng, Construction of three-dimensional nickel-vanadium hydrotalcite with ball-flower architecture for screen-printed asymmetric supercapacitor, *Appl. Surf. Sci.,* 2023, **615**, 156347.

7 A. G. El-Deen, M. K. Abdel-Sattar and N. K. Allam, High-performance solid-state supercapacitor based on Ni-Co layered double hydroxide@Co_3O_4 nanocubes and spongy graphene electrodes, *Appl. Surf. Sci.*, 2022, **587**, 152548.

8 X. Han, High mass-loading NiCo-LDH nanosheet arrays grown on carbon cloth by electrodeposition for excellent electrochemical energy storage, *Nano Energy*, 2021, **86**, 1060779

9 X. M. Yin, H. J. Li, R. M. Yuan and J. H. Lu, NiCoLDH nanosheets grown on MOF-derived Co_3O_4 triangle nanosheet arrays for high-performance supercapacitor, *J. Mater. Sci. Technol.*, 2021, **62**, 60–69.

10 Y. Liu, Y. Wang, C. Shi, Y. Chen, D. Li, Z. He, C. Wang, L. Guo and J. Ma, Co-ZIF

derived porous NiCo-LDH nanosheets/N doped carbon foam for high-performance supercapacitor, *Carbon*, 2020, **165**, 129–138.

11 R. R. Neiber, J. Kumar, R. A. Soomro, S. Karkus, H. M. Abo-Dief, A. K. Alanazi, A. A. Altalhia and Z. M. El-Bahy, $NiZnCoO_4/CoWO_4$ hybrid composite with improved electrochemical performance for supercapacitor application, *J. Energy Storage*, 2022, **52**, 104900.

12 C. H. Wu, Y. F. Wu, P. Y. Lee, S. Yougbaré and L.-Y. Lin, Ligand Incorporating Sequence-dependent ZIF67 Derivatives as Active Material of Supercapacitor: Competition between Ammonia Fluoride and 2-Methylimidazole, *ACS Appl. Mater. Interfaces*, 2022, **14**, 43180–43194.

13 K. Zheng, L. Liao, Y. Zhang, H. Tan, J. Liu, C. Li and D. Jia, Hierarchical NiCo-LDH core/shell homostructural electrodes with MOF-derived shell for electrochemical energy storage, *J. Colloid Interface Sci.*, 2022, **619**, 75–83.

14 D. Han, Y. Zhao, Y. Shen, Y. Wei, L. Mao and G. Zeng, Co_3O_4 nanowire@ultrathin Ni-Co layered double hydroxide core-shell arrays with vertical transfer channel for high-performance supercapacitor, *J. Energy Chem.*, 2020, **859**, 113887.

15 C. G. Wang, K. Guo, W. D. He, X. L. Deng, P. Y. Hou, F. W. Zhuge, X. J. Xu and T. Y. Zhai, Hierarchical $CuCo_2O_4$@nickel-cobalt hydroxides core/shell nanoarchitectures for high-performance hybrid supercapacitors, *Sci. Bull.*, 2017, **62**, 1122–1131.

16 G. Lei, D. Chen, Q. Li, H. Liu, Q. Shi and C. Li, NiCo-layered double hydroxide with cation vacancy defects for high-performance supercapacitors, *Electrochim. Acta*, 2022, **413**, 140143.